scientific reports

Check for updates

OPEN

Single-cell and multi-omics analysis identifies mitophagy-related biomarkers and therapeutic targets in ischemic stroke

Zhan Cao[1], Yingluan Wang[2], Mingjian Sun[1], Runyi Du[1], Xu Feng[1], Lin Wang[1], Ziyi Zhao[1] & Wei Sun[1]✉

Ischemic stroke (IS) remains a leading cause of death and disability, with limited effective treatments in the acute phase. Mitophagy, the selective degradation of damaged mitochondria, plays a crucial role in cellular homeostasis and survival during IS. However, its exact mechanisms in stroke pathophysiology remain unclear. This study utilized a multi-omics approach, integrating gene expression data from bulk and single-cell RNA sequencing, to investigate the role of mitophagy-related genes (MRGs) in IS. We identified differentially expressed MRGs (DE-MRGs) in IS using bioinformatics techniques, including weighted gene co-expression network analysis (WGCNA) and machine learning models, which led to the identification of five core biomarkers: SRPRB, ATP5J, LSM7, DEGS1, and TGDS. Validation via qPCR and analysis of immune cell infiltration further supported their relevance. Single-cell analysis revealed significant differences in mitophagy activity in microglial subpopulations, with ATP5J showing dynamic expression patterns linked to stroke-induced mitochondrial dysfunction. Additionally, pseudo-time analysis suggested a progressive shift from homeostatic to disease-associated microglial states. Our findings highlight the complexity of mitophagy regulation in IS and suggest that targeting mitophagy-related pathways, such as ATP5J, could provide novel therapeutic strategies for IS management.

Keywords Ischemic stroke, Mitophagy, Translational medicine, Microglia, Biomarkers

IS is the second leading cause of death and the third leading cause of disability worldwide. IS occurs when occlusion of cerebral blood vessels leads to reduced blood flow, resulting in tissue damage and neuronal death. Reperfusion therapy aims to restore blood flow and oxygen to the ischemic area. Clinically, intravenous thrombolysis and mechanical thrombectomy serve as the two primary reperfusion therapies, both constrained by strict time windows; the former carries a risk of intracranial hemorrhage and other complications, while the latter must be performed within 24 h of stroke onset[1,2]. Therefore, in-depth exploration of the pathophysiological mechanisms of IS is crucial for identifying new therapeutic strategies and providing a theoretical foundation for the treatment of IS.

The pathophysiological processes of IS involve various forms of cell death, including apoptosis, necrosis, and autophagy[3]. Among them, autophagy is an important intracellular degradation pathway that refers to the process by which cells wrap damaged or unwanted cellular components by forming autophagosomes, fusing them with lysosomes and then degrading and recycling them[4]. This process is regulated by PTEN-induced putative kinase 1 (PINK1) and Parkinson disease 2 (PARK2), both of which accumulate on the mitochondrial membrane and help stabilize mitochondrial depolarization[5]. Mitophagy, a selective form of autophagy, removes dysfunctional mitochondria for mitochondrial quality control[2]. The regulation of reactive oxygen species (ROS), calcium homeostasis, and energy supply are all critically dependent on mitochondria, and oxidative stress and cellular damage are made worse by their failure. When IS occurs, mitochondrial damage affects energy production, increases ROS levels, and facilitates the release of cytochrome c (Cyt c) to induce cell death. Reperfusion restores blood flow but can also trigger excessive ROS production, which can harm cells even more[6]. Thus, maintaining mitochondrial quality and quantity is essential for neuronal protection. Accordingly, mitophagy's prompt and effective removal of damaged mitochondria seems essential for IS cell survival[7]. Mitophagy has been shown

[1]Department of Neurology, The Second Affiliated Hospital of Harbin Medical University, Harbin 150086, China. [2]Department of Ophthalmology, The Second Affiliated Hospital of Harbin Medical University, Harbin 150086, China. ✉email: sunwei@hrbmu.edu.cn

to play a crucial role in cerebrovascular illnesses in recent years, and this suggests that it could be a promising treatment target for IS.

Bioinformatics is a multidisciplinary field that blends computational science and biology, using computational techniques and mathematical models to analyse large-scale biological data and reveal the laws of biological systems[8]. In neurology research, especially in complex therapeutic targets by analysing gene expression, co-expression networks and signaling pathways, providing a scientific basis for precision medicine and individualized treatment[9].

In this study, we integrate bulk and single-cell RNA sequencing with core molecular biology assays to delineate the contribution of MRGs to the pathogenesis of IS (Fig. 1). We specifically investigate how cell type–specific differential expression of MRGs shapes disease severity and heterogeneity, and we evaluate their potential as therapeutic targets. This approach is expected to refine diagnostic stratification and inform targeted interventions, ultimately improving clinical management and outcomes for patients with IS.

Results

Expression of DE-MRGs and immune infiltration analysis in IS patients

Datasets GSE16561 and GSE22255 were processed using the "sva" package to facilitate comprehensive data integration. Principal component analysis (Figure S2A, S2B) demonstrated successful elimination of batch effects. Subsequently, the merged dataset, GSEM, was used to assess the expression of MRGs in IS and control samples, identifying 19 DE-MRGs. The chromosomal locations of each gene are shown in the circos plot (Fig. 2C).

Compared to the control group, the expression of genes such as MAP1LC3B and UBE2D3 were higher in the IS samples, while genes like TOMM22, UBA52, and UBE2L3 were expressed at lower levels (Fig. 2A and B). We then performed correlation analysis of the DE-MRGs (Fig. 2D) to explore their role in IS. Notably, several DE-MRGs, such as TOMM22 and UBE2N, exhibited synergistic effects, while MAP1LC3A and FUNDC1 showed significant antagonistic effects.

Immune infiltration analysis was also performed to explore immune system differences between the two groups. The CIBERSORT algorithm revealed significant differences in the proportions of three immune cell types—CD8 + T cells, NK cells, and mast cells—between the control and IS groups (Fig. 2E). Correlation analysis between the DE-MRGs and immune cells showed that neutrophils and M1 macrophages were most strongly associated with mitophagy (Fig. 2F).

Identification of IS mitophagy clusters

We conducted consensus clustering analysis on the 19 DE-MRGs in order to comprehend their expression patterns in IS. The consensus index varied within a minimum range of 0.2 to 0.8 for K = 2 (Fig. 3A, B). The area under the cumulative distribution function (CDF) curve for K = 2–9 was determined by the difference between the two CDF curves (k and k-1) (Figure S3A). Additionally, consistency scores for all subtypes were approximately 0.9 only when K = 2 (Figure S3B). Based on the consensus matrix heatmap, the 59 patients were classified into two clusters: cluster 1 ($n = 23$) and cluster 2 ($n = 36$) (Figs. 3 C, S3C).

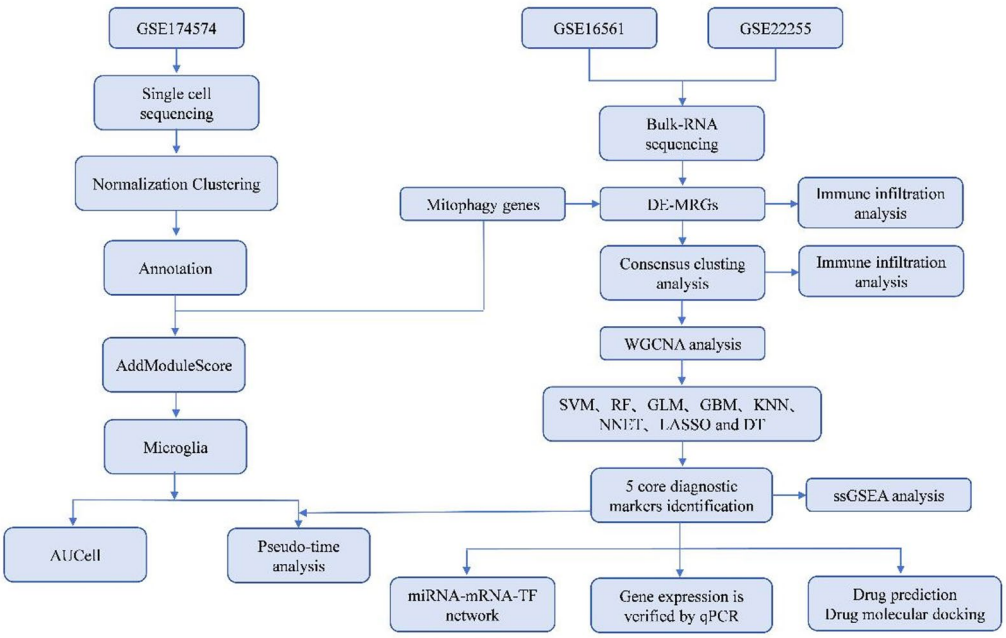

Fig. 1. Flowchart for predicting DE-MRGs in IS using bioinformatics analysis and experimental validation.

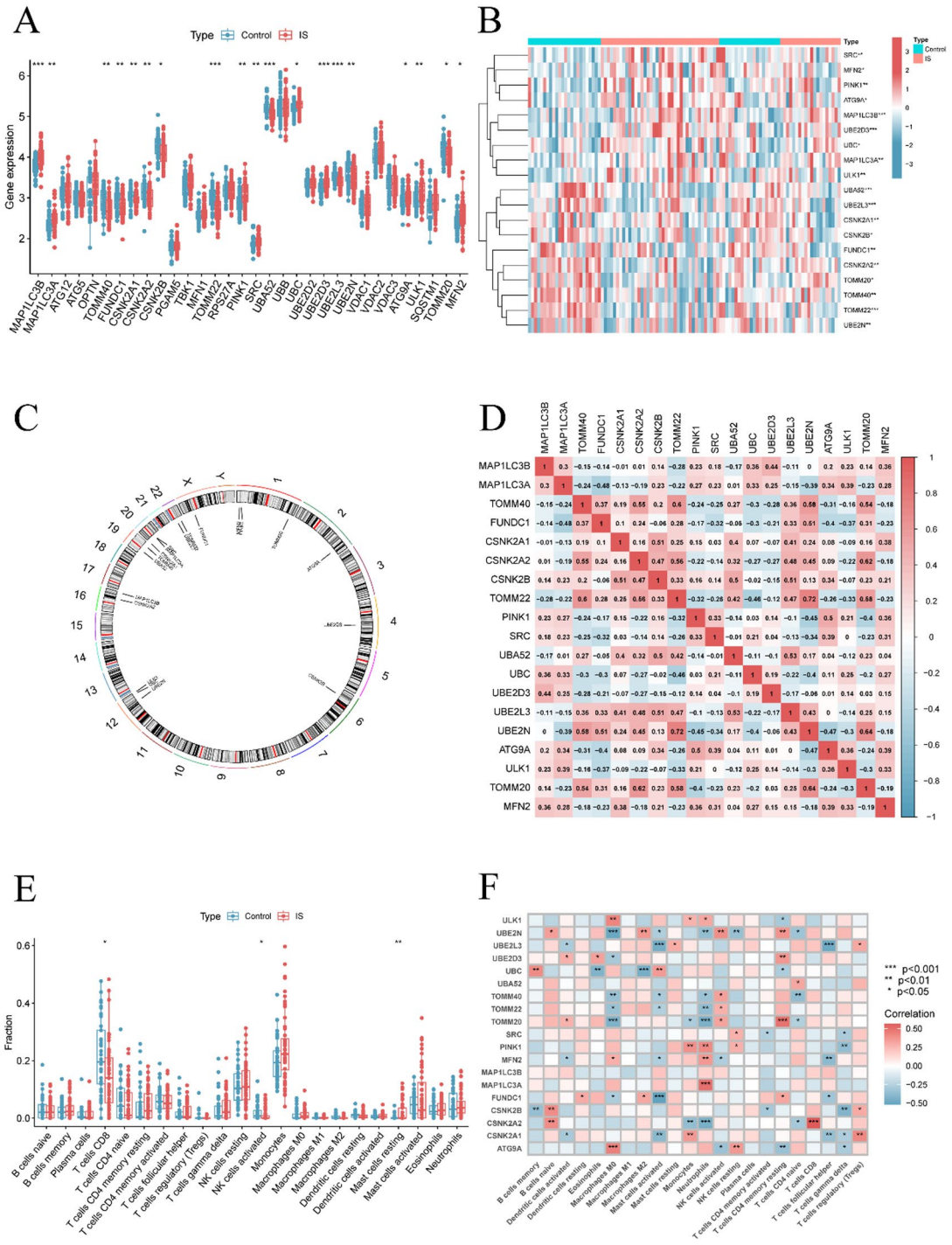

Fig. 2. Identification of DE-MRGs expression and immune infiltration analysis in IS. (**A**) Boxplots illustrating the expression levels of 19 DE-MRGs between IS and Control. (**B**) Heatmap displaying the expression patterns of 19 DE-MRGs. (**C**) Genosphere map of DE-MRGs. (**D**) Correlation analysis of DE-MRGs. (**E**) Boxplots showing differences in immune infiltration between IS and Control. (**F**) Correlation analysis between the 19 DE-MRGs and immune cells (*$p < 0.05$, **< 0.01, ***$p < 0.001$, ****$p < 0.0001$).

Next, we evaluated the expression differences of the 19 DE-MRGs between the two clusters. Cluster 1 exhibited high expression of genes such as MAP1LC3B, MAP1LC3A, UBC, CSNK2A1, and CSNK2B, while cluster 2 showed enhanced expression of TOMM40, FUNDC1, CSNK2A2, and TOMM22 (Fig. 3D).

We then examined the variations in immune cell infiltration between the two clusters, identifying different concentrations of four immune cell types. Resting NK cells, M0 macrophages, and neutrophils were found to be lower in cluster 2, although naive CD4 T cells and resting CD4 memory T cells were greater (Fig. 3E).

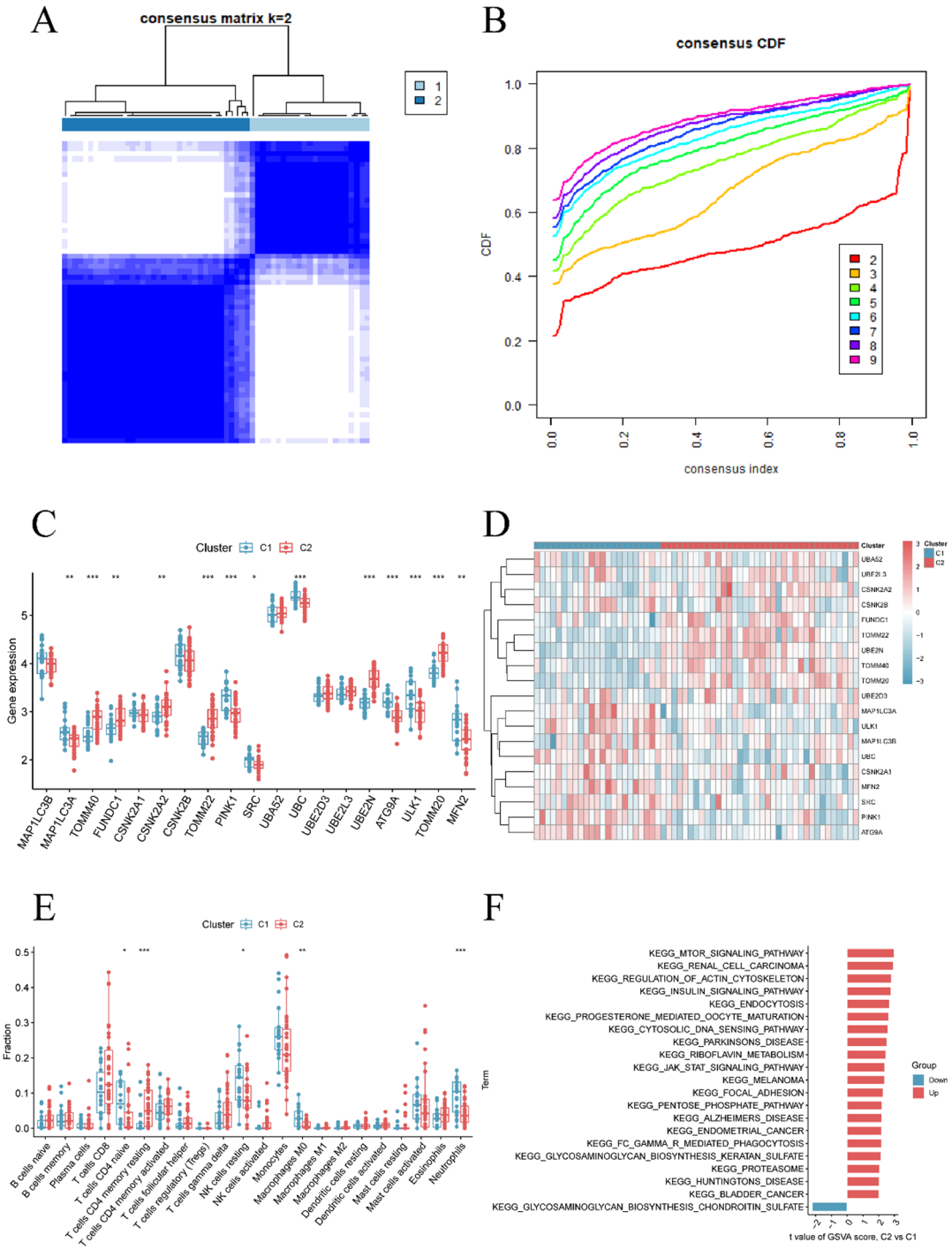

Fig. 3. Identification of mitophagy-related molecular clusters in IS. (**A**) Consensus clustering matrix for k = 2. (**B**) Representative CDF curves. (**C**) Boxplots displaying the expression of 19 DE-MRGs between the two mitophagy clusters. (**D**) Heatmap illustrating the expression patterns of 19 DE-MRGs. (**E**) Box plots showing the expression levels of immune cells between clusters. (**F**) GSVA-based KEGG pathway analysis between the two clusters. (*$p < 0.05$, **< 0.01, ***$p < 0.001$, ****$p < 0.0001$).

The two clusters' functional differences were discovered by additional GSVA analysis. Cluster 1 showed upregulation of the biosynthetic process of chondroitin sulfate, while cluster 2 displayed enhanced processes related to cell proliferation, differentiation, metabolism, cytoskeleton remodeling and regulation, insulin action, cell growth, and endocytosis (Fig. 3F).

Construction of weighted gene co-expression network and core module selection

WGCNA was applied to construct a co-expression network and identify gene modules associated with DE-MRGs in IS. The top 25% of genes with the highest variance in the GSEM dataset were selected for further analysis. With a soft threshold of 6, the scale-free R^2 reached 0.85, confirming the validity of the constructed co-expression modules (Fig. 4A, B). Multiple co-expression modules were identified using optimal dynamic tree cutting and hierarchical clustering methods (Fig. 4C). Notably, the brown module showed strong correlations with both clusters 1 and 2 ($p < 0.05$, Fig. 4D).

Next, we conducted enrichment analysis of the genes within the brown module using Metascape. The genes were mainly enriched in functions such as "ribosomal subunit", "mitochondrial membrane", "generation of ribonucleoprotein complexes", and "rough endoplasmic reticulum membrane" as well as pathways like "oxidative phosphorylation" (Fig. 4E).

Machine learning model construction

To identify key biomarkers with high diagnostic value, we constructed eight machine learning models based on the expression profile of the brown module from WGCNA, including SVM, RF, GLM, GBM, KNN, NNET, LASSO, and DT models. The "DALEX" package was used to interpret these models, and the residuals of each model in the training cohort were visualized. The residuals of the LASSO and SVM models were relatively low (Fig. 5A); GBM, SVM, and NNET displayed more stable distributions (Fig. 5B); GBM、RF and LASSO had a significant impact on the model performance (Figure S4). Additionally, ROC curves suggested that the best-performing model was NNET (AUC = 0.946), followed by LASSO (AUC = 0.941) and SVM (AUC = 0.905) (Fig. 5C). Based on these results, we selected the top five variables from the LASSO model (SRPRB, ATP5J, LSM7, DEGS1, and TGDS) as key gene biomarkers for subsequent analysis.

A nomogram was created using 103 IS examples to assess the LASSO model's predictive effectiveness (Fig. 5D). Calibration curves and DCA were employed to evaluate the predictive performance of the nomogram. The calibration curve indicated minimal error between the actual and predicted risks within the IS clusters (Fig. 5E). DCA further demonstrated that the nomogram exhibited high accuracy and could support clinical decision-making (Fig. 5F). Meanwhile, the diagnostic value of individual core biomarkers was also validated (Fig. 5G). At the same time, we also presented the expression of the core biomarkers in the GSEM (Fig. 5H).

SHAP analysis and qPCR validation of core diagnostic markers

The SHAP method explains the output of the best machine learning models by calculating the contribution of each variable to the prediction. The SHAP bar and bee plots (Fig. 5A, C) show that in the LASSO model, the factor with the highest contribution is DEGS1, followed by TGDS, with ATP5J, LSM7, and SRPRB contributing similarly. The SHAP dependency plot (Fig. 5B) demonstrates that DEGS1 is positively correlated with predicted risk and serves as the main risk factor in the model, while TGDS, ATP5J, LSM7, and SRPRB exhibit a clear negative correlation trend, suggesting they are protective factors. Analysis of the force plot for sample 1 (Fig. 5D) reveals that its predicted score (0.0355) is much lower than the baseline (0.575), primarily due to the dominant contribution of protective genes such as ATP5J, LSM7, and TGDS, which offset the influence of the risk gene DEGS1, thereby explaining the model's decision to classify it as low risk.

Finally, to validate the predictive performance of the core biomarkers, qPCR validation was performed using SH-SY5Y cells and peripheral blood from stroke patients (Fig. 6E-J). The results demonstrated that, compared to the control group, TGDS transcript levels were significantly decreased in both cellular and human peripheral blood samples (cells: Z = -2.561, $p = 0.003$; blood: $t = 11.143$, $p = 0.01$). DEGS1 transcript levels showed an upward trend (cells: t = -14.302, $p = 0.001$). However, SRPRB exhibited decreased transcript levels in the in blood (Z = -3.852, $p = 0.004$), whereas its transcript levels increased in the OGDR model (t = -7.298, $p = 0.003$). Furthermore, both ATP5J and LSM7 displayed downregulated transcript levels in the OGDR model ($t = 12.845$, $p < 0.001$; t = 14.474, $p < 0.001$), but were upregulated in the in blood (Z = -3.334, $p < 0.001$; Z = -2.099, $p = 0.036$).

Immune infiltration and enrichment analysis of five core biomarkers

We analyzed the correlation between five core biomarkers and immune cells (Fig. 7A). Among them, TGDS and LSM7 showed significant correlations with T cells CD4 memory resting (Fig. 7B, C).

Subsequently, we performed ssGSEA analysis to identify gene sets with statistically significant differences between the high-expression and low-expression groups of SRPRB, ATP5J, LSM7, DEGS1, and TGDS. The top five GO annotations and KEGG signaling pathways with the strongest positive and negative correlations are shown in Figures s5A-J.

The KEGG analysis of the pathways shared by the markers revealed that the core biomarkers were positively correlated with the protein export pathway and negatively correlated with pathways related to mature-onset diabetes in youth, linoleic acid metabolism, and olfactory transduction. TGDS, SRPRB, LSM7, and ATP5J were positively correlated with the ribosome pathway, RNA polymerase pathway, and DNA replication pathway, while negatively correlated with complement and coagulation cascade reactions.

The GO analysis of shared functional annotations for the markers indicated that ATP5J, LSM7, SRPRB, and TGDS were positively correlated with mitochondrial translation regulation and mitochondrial gene expression regulation. ATP5J, LSM7, and TGDS were positively correlated with rRNA methylation, while LSM7, SRPRB, and TGDS were negatively correlated with blood coagulation and fibrin thrombus formation.

Single-cell analysis of MRGs expression in IS

To deepen our understanding of how MRGs impact IS, we explored the GSE174574 dataset, which contains single-cell sequencing data from stroke mice, allowing us to assess mitophagy activity at single-cell resolution. Initially, the cells were clustered into 13 groups (Fig. 8A). These clusters were then categorized into seven distinct

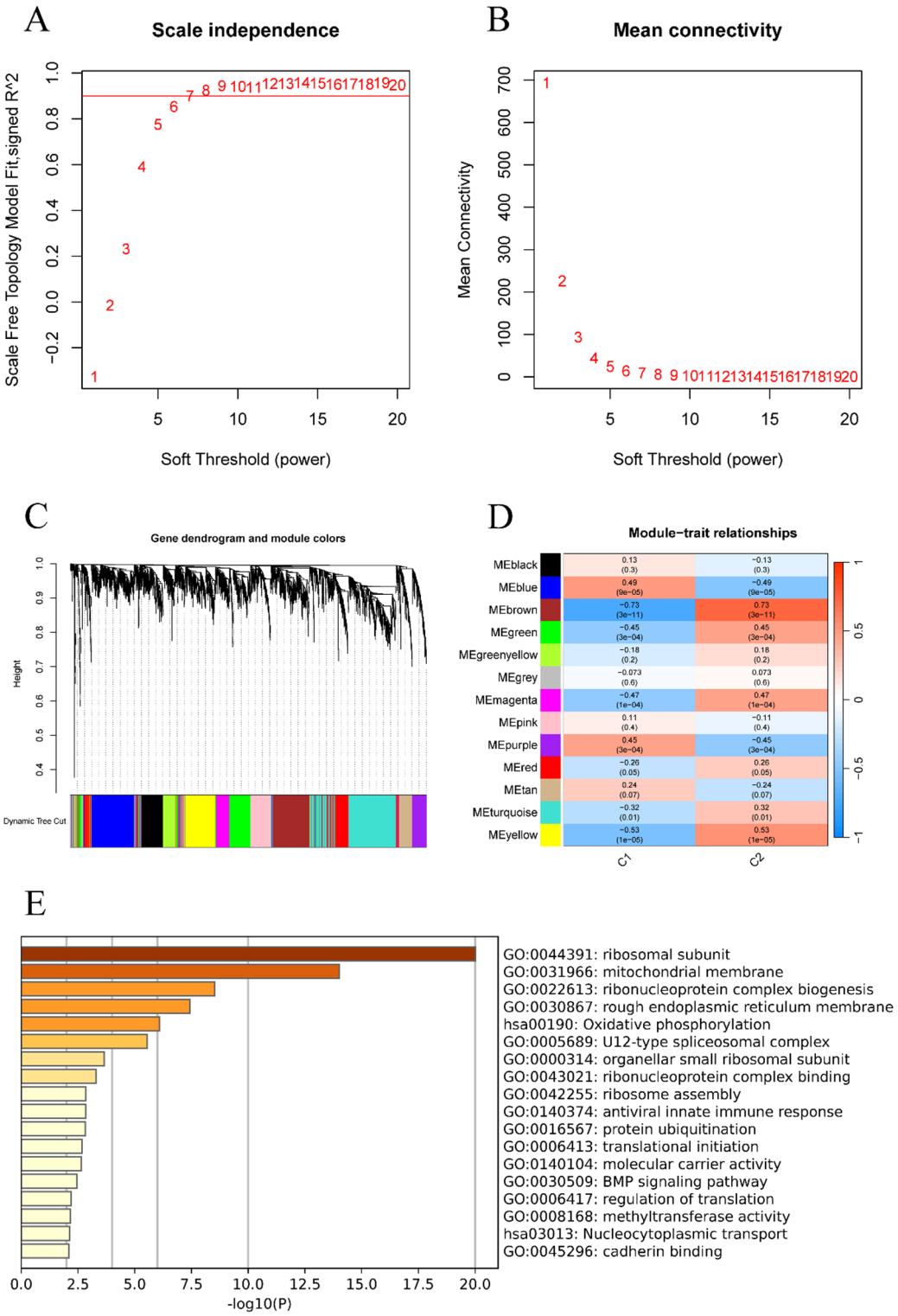

Fig. 4. Screening of gene modules and construction of co-expression networks. (**A**, **B**) Analysis of network topologies for different soft-thresholding powers based on the scale-free fit index (**A**) and mean connectivity (**B**). (**C**) Cluster dendrogram of co-expression modules. (**D**) Correlation analysis between module eigengenes and clusters, where each row represents a module and each column represents a cluster. (**E**) Metascape enrichment analysis for genes in the brown module.

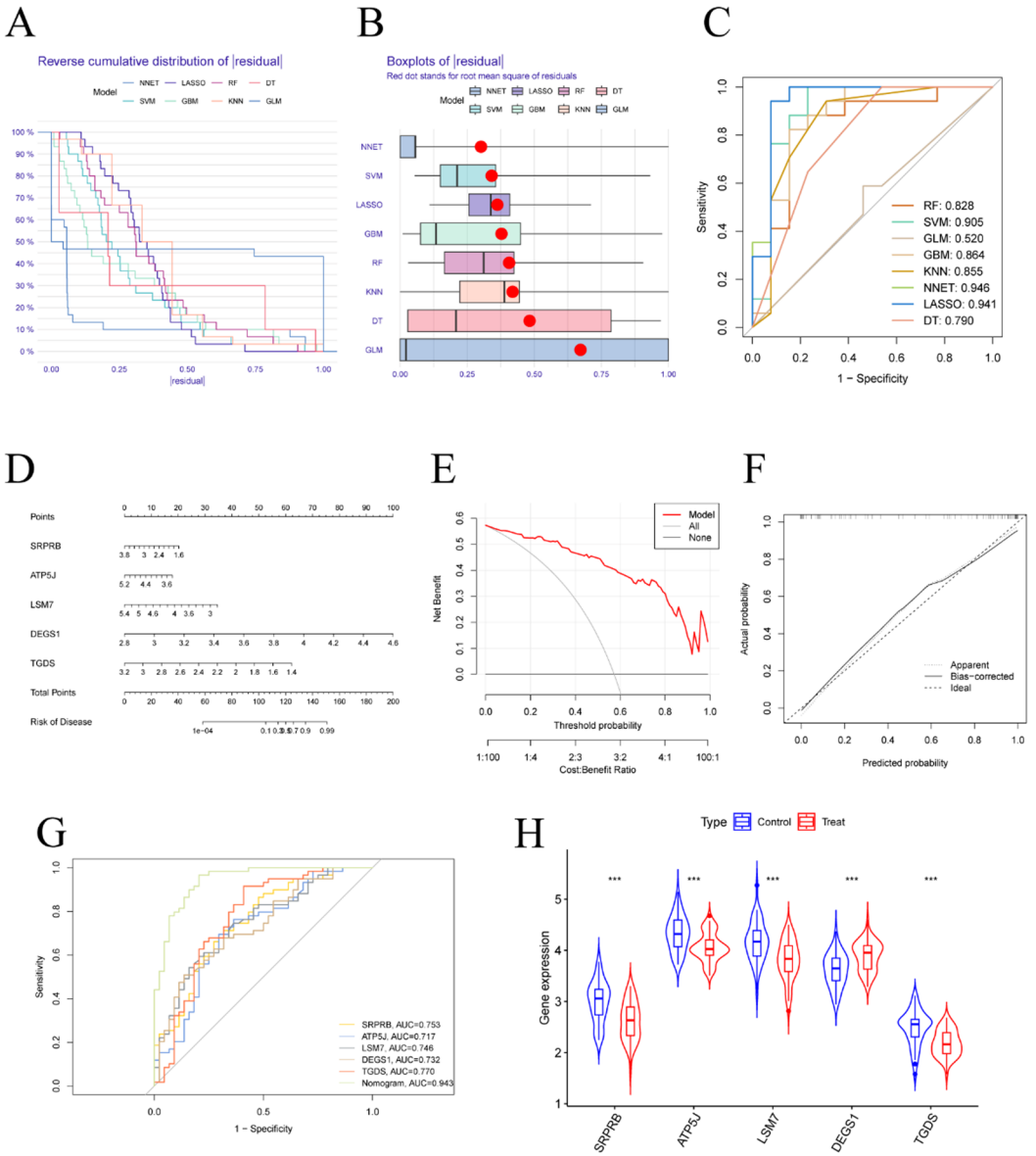

Fig. 5. Construction and evaluation of eight machine learning models and development of a predictive model. (**A**) Cumulative residual distribution for each machine learning model. (**B**) Boxplots displaying the residuals for each model, with the red dot representing the root mean square error (RMSE). (**C**) ROC analysis of the eight models based on 5-fold cross-validation in the testing cohort. (**D**) Development of a nomogram for predicting the risk of IS clusters using the 5-gene LASSO model. (**E**, **F**) Construction of the calibration curve (**E**) and DCA (**F**) to evaluate the predictive performance of the nomogram. (**G**) ROC analysis of the 5-gene LASSO model using 5-fold cross-validation. (**H**) The expression of core diagnostic markers in GSEM. (*$p < 0.05$, **< 0.01, ***$p < 0.001$, ****$p < 0.0001$).

cell populations based on marker gene expression: astrocytes, choroid plexus epithelial cells, endothelial cells, macrophages, microglia, monocytes, vascular smooth muscle cells, and oligodendrocytes (Fig. 8B). A top 10 gene heatmap was also constructed (Fig. 8C). We subsequently observed significant differences in microglia between the Sham and MCAO groups. Extensive analysis further revealed substantial variations in the mitochondrial autophagy scores of microglia between the Sham and MCAO groups (Fig. 8D).

To gain further insights, we performed dimensionality reduction and clustering of microglia, identifying four subpopulations: Mg1, Mg2, Mg3, and Mg4 (Fig. 8E-H). Mg1 was characterized by the expression of homeostatic genes (P2ry12, Siglech, Gpr34). Mg2 showed high expression of inflammatory and acute response genes, including Tnf, Ccl2, Ccl12, and Ier3, indicating an inflammatory, acute-response phenotype. Mg3 was defined by genes associated with disease-associated microglia (DAM), such as Lgals3, Adam8, Mmp12, and Cd44. Mg4 exhibited high expression of interferon response-related genes like Rsad2, Ifit1, Cxcl10, and Ifit2, suggesting that Mg4 is associated with an interferon response. Additionally, correlation analysis revealed that mitophagy levels

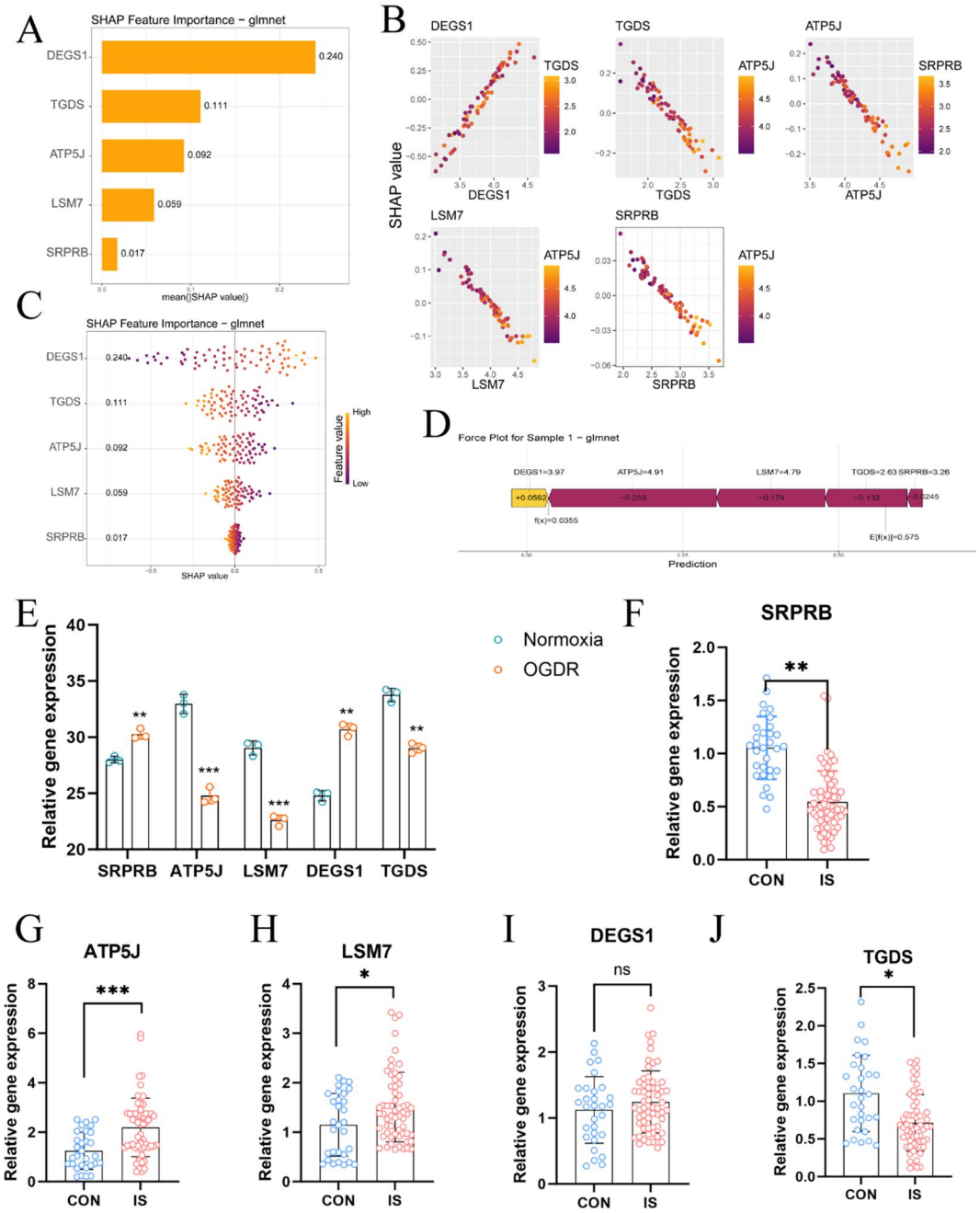

Fig. 6. SHAP analysis and qPCR validation of gene expression. (**A**) SHAP ROC curve showing model performance. (**B**) SHAP summary plot illustrating feature importance. (**C**) SHAP beeswarm plot showing the relationship between feature values and SHAP values. (**D**) SHAP bar plot showing the impact of genes on model predictions. (**E**) SHAP scatter plot showing the distribution of SHAP values. (**F**) SHAP dependence plots showing the relationship between genes and prediction outcomes. qPCR verification of the expression of core diagnostic markers in cellular(A) and human peripheral blood samples (**B**–**F**). (*$p < 0.05$, **< 0.01, ***$p < 0.001$, ****$p < 0.0001$).

were significantly and positively correlated with key pro-inflammatory factors, such as Il18 and Nlrp3 (Figure S6), suggesting a potential role for mitophagy in inflammatory regulation.

Subsequently, microglia were scored for mitochondrial autophagy and categorized into high and low mitochondrial autophagy microglia (Fig. 9A-B). We then examined the expression levels of core biomarkers in microglia (Fig. 9C). Based on the qPCR results, as well as the findings from conventional transcriptomic and single-cell data, we identified Atp5j as the best candidate gene. Building on this, we performed pseudo-time analysis and constructed a developmental trajectory resembling a dendritic structure, predicting that microglia progress from the stable state of Mg1 to the acute response state of Mg2, and eventually to the disease-associated state of Mg3(Fig. 9D-E). During the initial and middle phases of this trajectory, Atp5j exhibited an

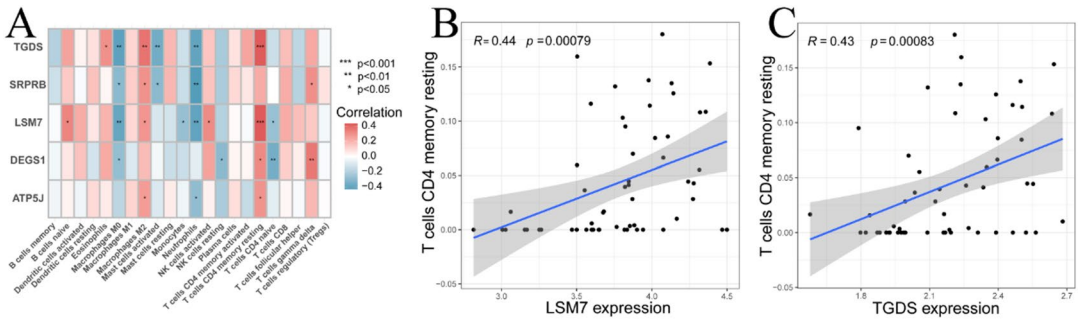

Fig. 7. Analysis of immune infiltration and ssGSEA of five core biomarkers. (**A**) The correlation analysis between five core biomarkers and immune cells. Among them, LSM7 (**B**) and TGDS (**C**) correlated most strongly with T cells CD4 memory resting.

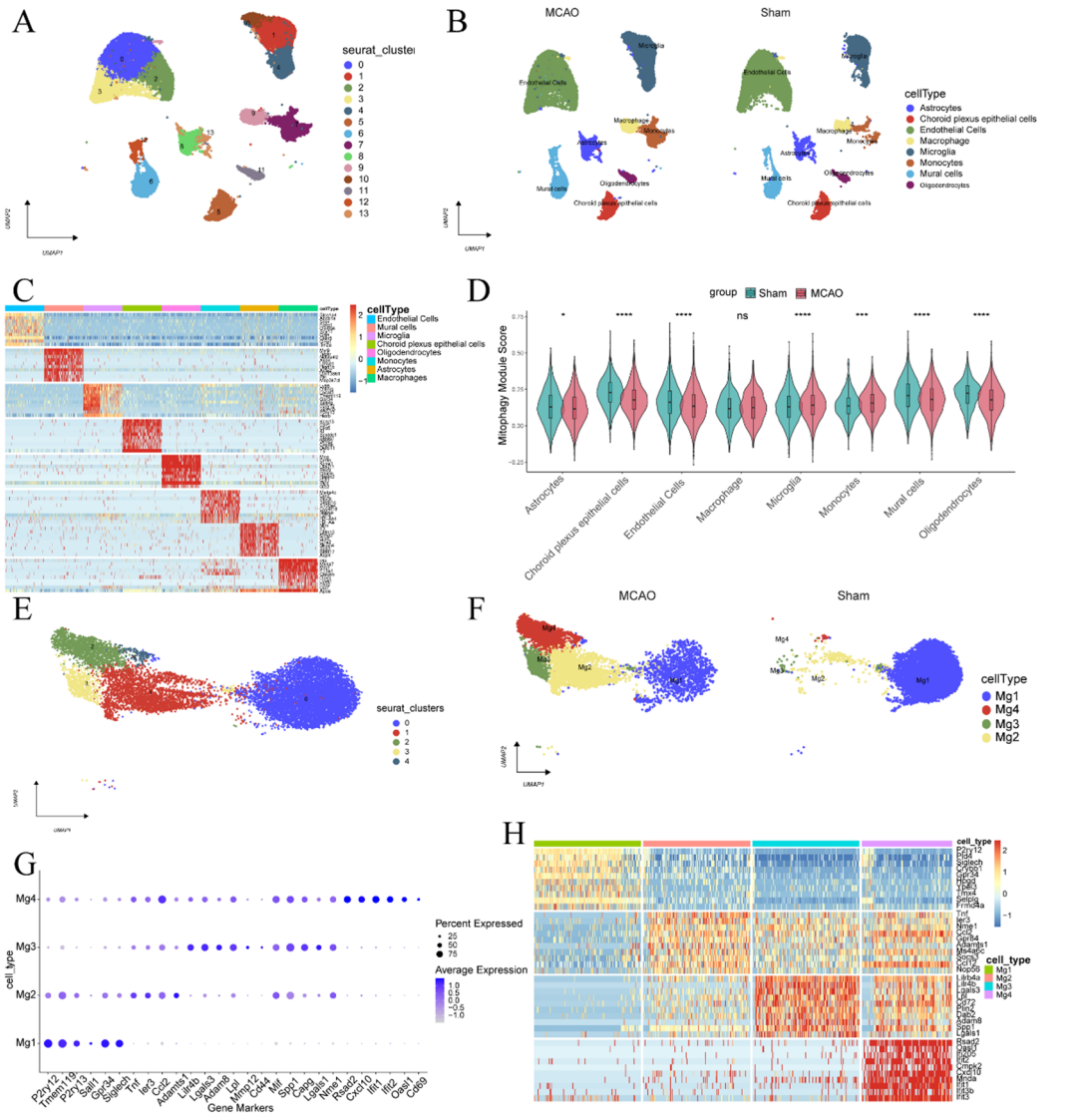

Fig. 8. Single-cell analysis of mitophagy activity in IS. (**A**) Cell clusters in the IS dataset GSE174574. (**B**) Annotated cell populations. (**C**) Heatmap of top 10 genes in different cell types. (**D**) Mitochondrial autophagy scores between Sham and MCAO groups. (**E**) Cell clusters of microglia. (**F**) Annotation of microglial subpopulations. (**G**) Bubble plot of marker genes for the subpopulations. (**H**) Heatmap of top 10 genes in different cell subpopulations.

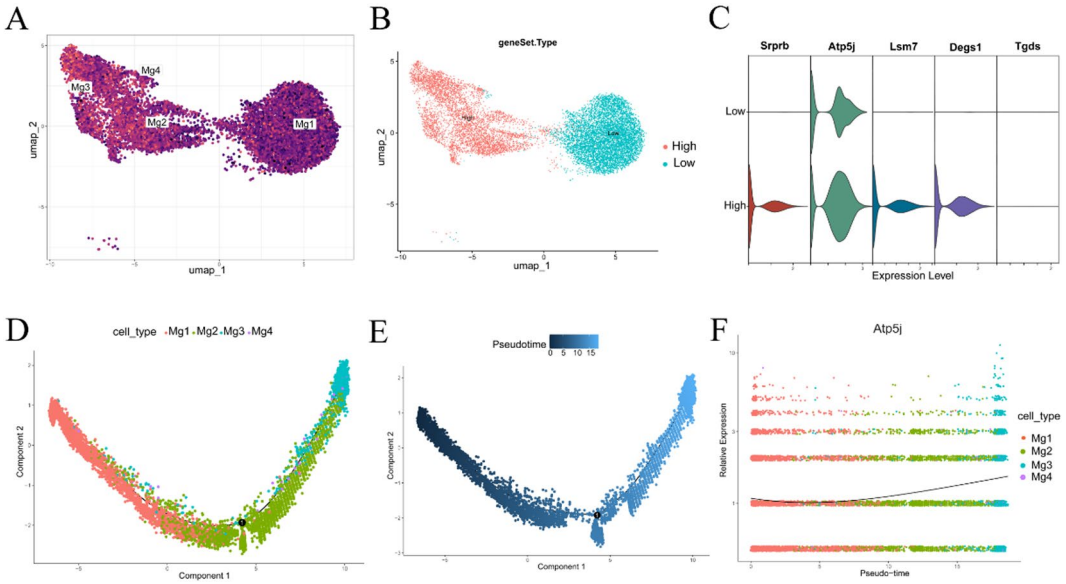

Fig. 9. (**A**, **B**)AUCell scoring divided into high and low expression groups. (**C**) Expression variation of core biomarkers between high and low groups. (**D**) Monocle-based pseudo-time trajectory colored by pseudo-time. (**E**) Monocle-based pseudo-time trajectory colored by cell type. (**F**) Expression levels of ATP5J in different cell types during pseudo-time analysis.

increasing trend as the trajectory developed(Fig. 9F), further confirming the critical role of microglia and Atp5j in mitochondrial autophagy.

Discussion

In the early stage of IS, interruption of cerebral blood flow leads to hypoxia in brain cells, subsequently causing mitochondrial dysfunction. Mitochondria, as the central organelles for cellular energy production, exhibit reduced ATP synthesis and excessive ROS generation under hypoxic conditions. The accumulation of ROS further exacerbates mitochondrial damage, triggers the opening of the mitochondrial permeability transition pore, and ultimately induces cell apoptosis and necrosis[10,11]. Mitophagy, the selective autophagic degradation of damaged mitochondria, plays a critical role in maintaining mitochondrial homeostasis. Moderate activation of mitophagy can reduce ROS accumulation, restore mitochondrial function, and alleviate IS-induced cellular injury[12–14]. The threshold between moderate and excessive mitophagy is not absolute but likely determined by a dynamic balance among injury intensity/duration, mitophagy pathway activation, autophagic flux, and mitochondrial biogenesis. Transient, controllable injury tends to be protective, while prolonged or intense damage may exceed the protective window, leading to net mitochondrial depletion and energy failure[2,15]. Therefore, given the dual role of mitochondrial autophagy in the survival and death of neurons after stroke, it is of great significance to conduct in-depth research on its mechanism.

To further explore the role of mitophagy in IS, we conducted systematic bioinformatics analyses to study and validate the expression patterns of MRGs and their potential connections with the pathological mechanisms of IS[16].

MAP1LC3B (microtubule-associated protein 1 light chain 3β) regulates autophagy and plays a key role in mitochondrial quality control, energy homeostasis, and ROS clearance. After stroke, ischemia activates microglia and upregulates MAP1LC3B, promoting autophagosome formation to counter neuronal damage[17,18]. UBE2D3 (ubiquitin-conjugating enzyme E2 D3) works with Park2 to ubiquitinate damaged mitochondrial proteins, initiating mitophagy. Reduced UBE2D3 expression impairs mitophagy efficiency[19]. TOMM22 (translocase of outer mitochondrial membrane 22) influences mitophagy via the PINK1-Park2 pathway. Downregulation of TOMM22 disrupts mitochondrial protein homeostasis and worsens neuronal injury post-stroke[20]. UBA52 (ubiquitin precursor protein) generates ubiquitin for Park2-mediated chain synthesis. Insufficient UBA52 limits ubiquitination efficiency and weakens mitophagy[21]. UBE2L3 (ubiquitin-conjugating enzyme E2 L3) aids Park2 in mitochondrial protein ubiquitination, and its downregulation impairs autophagosome recognition of damaged mitochondria[19]. The PINK1-Park2 pathway clears dysfunctional mitochondria, improving neuronal survival after ischemia-reperfusion injury[14]. Dysregulation of TOMM22, UBE2D3, UBA52, and UBE2L3 disrupts this pathway, leading to mitochondrial quality control imbalance and exacerbating neuronal damage post-stroke.

We also looked at the immune cell abundance differences between IS and control patients, and we discovered that IS patients had higher levels of mast cell and NK cell infiltration. Following the onset of IS, the nervous system is damaged, and cell death coupled with local inflammatory responses leads to a series of changes in immune reactions. NK cells and mast cells are recruited, resulting in increased infiltration. NK cells are recruited early during brain ischemia and accumulate around ischemic neurons. In experimental stroke models, NK cell accumulation peaks as early as 3 days post-ischemia and exacerbates neuronal damage[22,23]. Through the release

of mediators, mast cells can attract other immune cells to intensify the inflammatory response and encourage hemorrhage development, vasogenic edema, and disruption to the blood-brain barrier[24].

Furthermore, we identified two distinct clusters based on DE-MRGs expression using unsupervised clustering technique. GSVA analysis of the clusters revealed that the metabolic characteristics of cluster 1 were more associated with inflammation and structural protection, while cluster 2 reflected enhanced cellular activity and potential adaptive mechanisms for repair. We subsequently performed WGCNA on the clusters and identified the most strongly correlated brown module, which contained 111 genes. Enrichment analysis of the brown module also reflected the central role of mitochondrial functions (e.g., energy metabolism, protein synthesis) in the pathological process of IS.

In this study, we chose LASSO as the best model and identified five core biomarkers: SRPRB, ATP5J, LSM7, DEGS1, and TGDS. In the machine learning screening, the five-gene combined model (LASSO) demonstrated high ROC-AUC values (>0.90), and qPCR further confirmed their differential expression in the OGDR model ($p < 0.05$), supporting their clinical diagnostic potential.

SRPRB (signal recognition particle receptor subunit β) is primarily involved in co-translational targeting of nascent peptides to the endoplasmic reticulum (ER) membrane[25]. In tumor cells, SRPRB upregulation may promote apoptosis by inhibiting NF-κB activation[26]. Emerging evidence indicates that ER stress regulates PINK1/Parkin-dependent mitophagy via the PERK/ATF4/CHOP axis, and that ER-mitochondria contact sites (MAMs) play critical roles in spatially organizing PINK1/Parkin signaling and maintaining Ca^{2+} homeostasis[27]. Thus, although SRPRB is not a direct mitophagy receptor, its ER-localized function suggests it could indirectly influence mitophagy by modulating ER-mitochondria crosstalk and ER stress responses. The divergent expression of SRPRB between our OGDR model (upregulated) and patient peripheral blood (downregulated) may reflect temporal and spatial differences between acute in vitro stress and systemic immune signals in vivo, warranting further validation in brain tissue.

ATP5J, a structural component of mitochondrial complex V (ATP synthase), is directly involved in oxidative phosphorylation, membrane potential (ΔΨm) maintenance, and cristae integrity. These mitochondrial parameters serve as upstream triggers for PINK1 accumulation on the outer mitochondrial membrane and subsequent Parkin recruitment, initiating canonical PINK1/Parkin-mediated mitophagy[28]. In brain injury models, ATP5J upregulation in microglia exacerbates mitochondrial dysfunction and promotes neuroinflammation[29], while in cerebral ischemia-reperfusion, PINK1/Parkin/p62-mediated mitophagy is temporally activated[28]. Additionally, ischemia-induced energy stress activates AMPK, which regulates mitophagic flux via ULK1 and mTOR[30]. Therefore, the bidirectional expression changes of ATP5J observed in our study (down in OGDR, up in patient blood) may reflect distinct phase-specific responses: acute energy crisis driving AMPK-mediated mitophagy initiation versus chronic inflammatory states involving metabolic reprogramming.

LSM7, a core component of the conserved Lsm1-7 complex, functions as an RNA metabolism/stability regulator. Under nutrient deprivation, Lsm7 forms a complex with Pat1 to promote the accumulation of autophagy-related gene (ATG) mRNAs, thereby facilitating autophagic program initiation[31]. Although mitophagy employs specialized machinery (PINK1/Parkin, BNIP3/NIX), its execution still depends on the core autophagic apparatus (ULK1 complex, LC3 lipidation, lysosomal flux), which is regulated by AMPK activation and mTOR inhibition in response to energy stress[30]. Thus, LSM7 may influence mitophagy by modulating the supply of core ATG products, thereby affecting the "execution capacity" of mitophagy under ischemic stress. The inconsistent expression patterns across models likely reflect temporal differences in autophagic demand and transcriptional regulation.

DEGS1, a sphingolipid Δ4-desaturase involved in ceramide synthesis, has recently been identified as a resident enzyme of mitochondria-associated ER membranes (MAMs) that is essential for MAM integrity[32]. Disruption of DEGS1 may impair MAM stability, indirectly affecting PINK1/Parkin pathway efficiency and autophagosome formation. Moreover, sphingolipid/ceramide metabolism itself regulates mitochondrial homeostasis and mitophagy; for instance, ceramide accumulation under PINK1 deficiency can induce mitophagy accompanied by fatty acid β-oxidation defects, and BNIP3 has been implicated in ceramide-induced autophagy/mitophagy[33]. The consistent upregulation of DEGS1 in both our OGDR model and stroke patient blood suggests a common pathological link involving sphingolipid metabolic remodeling, increased MAM/mitochondrial quality control stress, and compensatory or passive activation of mitophagy pathways.

TGDS, a UDP-glucose 4,6-dehydratase-like protein, has recently been shown to generate UDP-4-keto-6-deoxyglucose, which sustains the UXS1 catalytic cycle under NAD^+-depleted conditions and influences glycosaminoglycan synthesis[34]. This implicates TGDS in cellular redox and energy cofactor homeostasis. During ischemic stress, cerebral ischemia-reperfusion is accompanied by NAD^+/ATP metabolic remodeling, and AMPK activation (via ULK1 and mTOR) orchestrates the intensity and direction of autophagy/mitophagy initiation[30]. The consistent downregulation of TGDS in both our OGDR model and patient blood may reflect constrained glucose metabolism and cofactor supply under ischemic stress, leading to passive AMPK activation and increased pressure on mitochondrial quality control, rather than direct engagement with PINK1/Parkin or BNIP3/NIX.

In this study, SRPRB, LSM7, and ATP5J exhibited opposite expression trends between the OGDR model and patient peripheral blood samples, whereas DEGS1 and TGDS showed consistent trends across both. These discrepancies likely reflect differences in temporal regulation between the acute versus subacute/chronic phases, tissue/cell-type-specific expression patterns, and the inherent divergence between in vitro models and the in vivo microenvironment. As an in vitro system, the OGDR model primarily simulates acute ischemic hypoxia and short-term reperfusion injury, capturing the "immediate transcriptional response" of cells within a timeframe of hours[35]. Such acute responses mainly involve rapid mechanisms including intracellular energy metabolism, stress signaling, and translational regulation. In contrast, clinical samples are typically collected over a broader post-stroke time window, and their gene expression profiles represent the cumulative result of temporal

dynamics, influenced by multiple factors such as immune cell infiltration, amplification of inflammatory signals, and systemic metabolic reprogramming. Furthermore, the OGDR model lacks key physiological factors present in vivo, including inflammatory cytokines, vascular disruption, and immune cell recruitment, all of which play critical roles in clinical stroke. Therefore, the observed directional differences in gene expression are likely attributable to these biological discrepancies.

Subsequently, an ssGSEA analysis was performed on the five core biomarkers, revealing that the positively correlated pathways commonly associated with these biomarkers were mainly concentrated in cellular metabolic processes and genetic information transmission, while the negatively correlated pathways were focused on metabolism and immune regulation. Functional analysis of these shared pathways showed that the five biomarkers were positively correlated with mitochondrial function (e.g., translation regulation, gene expression, and RNA processing) and ribosome biogenesis (e.g., RNA modification); they were negatively correlated with processes such as blood coagulation, fibrinolysis, and cell differentiation. TGDS, SRPRB, LSM7, and ATP5J were found to be involved in immune system and coagulation processes, with SRPRB showing a strong correlation with immune function. This finding is consistent with our immune cell correlation analysis of the core biomarkers. These results suggest that core biomarkers may influence the onset and progression of IS by regulating mitochondrial functions (such as energy metabolism and RNA translation) and the immune system (such as coagulation cascade).

In this study, we also explored the role of mitophagy in microglia at the single-cell level following stroke. By scoring the levels of mitophagy, we observed significant differences in mitophagy activity among microglial clusters post-stroke. Specifically, microglial clusters Mg1 (homeostatic microglia), Mg2, and Mg3 (DAM) exhibited distinct mitophagy characteristics. Stroke induced microglial activation, and compared to Mg1, the mitophagy levels in Mg2 and Mg3 were significantly elevated, indicating a compensatory response to stroke-induced mitochondrial dysfunction. Studies suggest that activated microglia can enhance mitophagy, alleviating neuroinflammation and neuronal defects[36].

Pseudo-time analysis of microglial clusters revealed their developmental trajectory, showing a progressive transition in mitotic activity from Mg1 to Mg3. Notably, mitophagy-related genes, such as ATP5J, were expressed at higher levels in Mg2 and Mg3 compared to Mg1, suggesting that these genes play a crucial role in the pathophysiology of stroke. ATP5J is a key gene in mitochondrial function and mitophagy, and its dynamic expression pattern in these microglial subtypes highlights its potential role in regulating mitophagy and cellular responses after stroke.

In conclusion, these findings underscore the complexity of autophagy regulation in microglia during stroke. While the elevated mitophagy in disease-associated microglia (Mg2, Mg3) plays a protective role in enhancing mitochondrial quality control, maintaining a balance is critical, as excessive mitophagy may lead to further mitochondrial degradation and exacerbated neuroinflammation[37]. However, it is important to note that the regulation of mitophagy and its related genes exhibits significant cell-type specificity. Our single-cell analysis indicates that microglia are key participants in the dynamic changes of mitophagy after stroke, whereas our in vitro validation experiments were performed using neuronal cells. Neurons and microglia possess fundamentally distinct metabolic profiles and stress responses: neurons prioritize maintaining energy homeostasis under ischemic stress[38], while microglia are more inclined toward immune activation and phagocytic clearance[39]. These inherent differences may lead to divergent expression patterns of the same gene under identical pathological conditions. Therefore, although targeting mitophagy-related pathways such as ATP5J may offer a promising therapeutic strategy for stroke, future research should consider cell-type specificity and validate relevant findings in appropriate cellular models.

This study has several limitations. First, regarding the validation methods, we primarily relied on peripheral blood mRNA detection and in vitro cellular models, which cannot directly reflect the dynamic changes of mitophagy within the brain parenchyma. Second, due to the cross-sectional study design, we were unable to establish a definitive causal relationship between mitophagy-related gene expression and the pathogenesis of stroke. Furthermore, the data used in this study were all sourced from public databases; due to the retrospective nature of these data, detailed information such as the patients' treatment conditions and medication usage could not be obtained. Consequently, we were unable to systematically adjust for potential treatment-related confounding factors as would be possible in a prospective clinical study. In view of this, future translational research should conduct validation in larger, better-characterized population cohorts. Finally, the specific regulatory mechanisms of these core genes in the occurrence and development of stroke still need to be elucidated through in-depth, multi-dimensional functional experiments.

Materials and methods

Data collection and preprocessing, identification of DE-MRGs expression

Two IS datasets (GSE16561 and GSE22255) were found from the GEO database. Forty MRGs were identified from the Reactome database (https://reactome.org/)) by directly downloading all genes annotated to the 'Mitophagy' pathway without applying any additional inclusion/exclusion criteria. The datasets were merged into a single dataset, named GSEM, with detailed information about the dataset provided in Table 1. After normalizing and annotating the raw data, batch effects were eliminated from the combined dataset using the "SVA" package. The "Limma" package was used to analyze DE-MRGs between the IS and control groups in the GSEM dataset[40].

Consensus clustering analysis and WGCNA

The "ConsensusClusterPlus" program was used to conduct a consensus clustering analysis of GSEM[41]. The median absolute deviation was used to categorize IS samples. The ideal number of clusters was then ascertained using unsupervised consensus clustering[42].

Datasets	Platform	Organism	Control	IS	Sequencing type
GSE16561	GPL6883	Homo sapiens	24	39	mRNA
GSE22255	GPL570	Homo sapiens	20	20	mRNA
GSE174574	GPL21103	Mus musculus	3	3	scRNA-seq

Table 1. Basic information of the datasets.

The "WGCNA" program was used to perform WGCNA[42]. The "pickSoftThreshold" function was used to determine the optimal weighting parameter value in the adjacency function, and this value was used as the soft threshold for the subsequent network development[43]. A weighted adjacency matrix was created, and gene modules formed via hierarchical clustering based on the 1-TOM dissimilarity matrix[44]. Every module was given a distinct color identification, and the expression profile of the entire module was represented by the module eigengene. The module-consensus clustering cluster relationship represented module significance, while gene significance described the correlation between the gene and the mitophagy cluster.

Building prediction models using a variety of machine learning techniques

The machine learning prediction models used were Random Forest (RF), Support Vector Machine (SVM), Generalized Linear Model (GLM), Gradient Boosting Machine (GBM), k-Nearest Neighbors (KNN), Neural Network (NNET), Least Absolute Shrinkage and Selection Operator (LASSO), and Decision Tree (DT)[45,46].

We used the "caret" package to divide the data into a training set (70%) and a testing set (30%). Within the training set, we performed 5-fold cross-validation to tune hyperparameters and train eight machine learning algorithms. The "DALEX" package was then applied to interpret the models by analyzing residual distributions and feature importance. The "pROC" package was utilized to generate ROC curves and calculate AUC values for model performance evaluation on the testing set.

Nomogram construction and validation

The "RMS" program was used to create a nomogram for individualized risk assessment and forecasting. A particular score was assigned to each predictor variable, and the risk for each individual was determined by adding up these individual scores. Decision Curve Analysis (DCA) and calibration curves were used to assess the nomogram's predictive ability[47].

SHAP analysis

We used the "shapviz" package to perform SHAP analysis in order to assess the contribution of features to the model's predictions. A machine learning model was trained on gene expression data, and SHAP values were computed to explain the importance of each gene. SHAP summary plots, swarm plots, and dependence plots were employed to visualize the impact of genes on the model's predictions.

Analysis of immune cell infiltration and enrichment

Using the CIBERSORT algorithm, the relative abundance of 22 immune cell types in GSEM was estimated using the LM22 signature matrix and gene expression data. CIBERSORT used Monte Carlo sampling to determine the p-values for each sample's deconvolution. Only samples with $p < 0.05$ were deemed to have accurate immune cell compositions after the relative proportions of each of the 22 immune cell types were adjusted to total to 1[48]. For in-depth immune infiltration analysis, the "IOBR" package was used to explore the interactions between DE-MRGs, consensus clustering clusters, biomarkers, and various immune cell types[49].

To investigate pathway differences between the consensus clusters, Kyoto Encyclopedia of Genes and Genomes (KEGG) pathway analysis was conducted using Gene Set Variation Analysis (GSVA) on the consensus clustering clusters[50]. The most highly connected co-expression modules were then subjected to KEGG enrichment analysis and Gene Ontology (GO) using Metascape. The ssGSEA was performed on the core biomarkers.

Basic analysis workflow of scRNA-seq data

In the quality control process of our scRNA-seq data, we retained cells that expressed at least 300 genes and had mitochondrial gene counts lower than 20% of the total gene count. We used the "DoubletFinder" tool to computationally detect cell doublets, with an expected doublet rate of 7.5% as an input parameter. Cells identified as "Doublets" were excluded. Dimensionality reduction and clustering analysis were performed using the "Seurat" package. To address potential batch effects that may affect the accuracy of single-cell analysis, we applied the "harmony" package for batch effect correction, focusing on the top 2000 variable genes using default parameters. Clustering was conducted using the "FindNeighbors" and "FindClusters" functions in Seurat, which implement a shared nearest neighbor (SNN)-based clustering algorithm optimized by modularity on the selected principal components, with a resolution set to 0.4. Mitochondrial autophagy scores for cell types were calculated using "AddModuleScore", and mitochondrial autophagy scoring for microglial subpopulations was performed with "AUCell". For differential gene expression analysis, we used the "FindMarkers" function with default settings. Secondary clustering of microglia was conducted using a similar approach, maintaining a resolution of 0.4. "Monocle2" was used for pseudo-time analysis of microglial subpopulations.

Core biomarkers validation

Vitro validation

The SH-SY5Y cells were incubated at 37 °C with 5% CO2 for 24 h. When cells reached 70%-80% confluence, they were subjected to 4 h of hypoxia in a three-gas incubator (Thermo, MA, USA) with no-glucose medium, using a gas mixture of N2 (94%), O2 (1%), and CO2 (5%). Afterward, the cells were transferred to normal glucose-containing medium and cultured under normal oxygen conditions (21% O_2, 5% CO_2) for 12 h to simulate reperfusion. Cell viability was then assessed by CCK-8 assay (Figure S1).

Study participants

A total of 60 patients with acute stroke hospitalized in the Department of Neurology, the Second Affiliated Hospital of Harbin Medical University between January and July 2025 were recruited as the experimental group (IS group). Concurrently, 30 non-stroke patients hospitalized in the same department during this period served as the control group. 5 mL of freshly collected anticoagulated peripheral blood (EDTA-K2 tubes) was drawn within 2–4 h after admission.

Inclusion criteria

IS Group: (1) Head CT or MRI indicates the presence of a new infarction focus. (2) Hospitalization ≤ 72 h post-symptom onset (extended window cases require perfusion mismatch. (3) NIHSS 4–25.

Control Group: (1) Age/sex-matched to IS group. (2) Hospitalized for non-stroke conditions (e.g., migraine, dizziness) with normal brain MRI/CT.

Exclusion criteria

(1) Active cancer, severe organ failure (eGFR < 30 or Child-Pugh C). (2) Current anticoagulation (INR > 1.7) or contraindications to thrombolysis. (3) Missing baseline NIHSS or imaging timestamps.

Total RNA was extracted using Trizol reagent (Ambion, Austin, Texas, U.S.) according to the manufacturer's protocol, and its concentration was measured with a NanoDrop spectrophotometer (N50). Reverse transcription was performed with a standard PCR instrument (Servicebio, Wuhan, China), and the cDNA was diluted 5–20 times using RNase/DNase-free water. QPCR amplification was conducted, and relative mRNA expression was calculated using the $2^{-\Delta\Delta Ct}$ method. The primer sequences used are listed in Table S1.

Statistical methods

All raw data were processed using *R* (version 4.2.1). To assess significant differences between two independent groups, *t*-tests or Wilcoxon rank-sum tests were used based on the data distribution. *P*-values were calculated as two-sided, with statistical significance set at $p < 0.05$.

Data availability

This paper analyzes existing, publicly available data, accessible at GEO Database: GSE16561 and GSE22255. qPCR validation data supporting this study are included in the Supplementary Materials. This paper does not report original code. Requests for further information and resources should be directed to and will be fulfilled by the lead contact, Wei Sun ([sunwei@hrbmu.edu.cn](mailto: sunwei@hrbmu.edu.cn)).

Received: 21 September 2025; Accepted: 4 March 2026
Published online: 06 March 2026

References

1. Sun, F. et al. No-reflow after recanalization in ischemic stroke: From pathomechanisms to therapeutic strategies. *J. Cereb. Blood Flow. Metab.* **44** (6), 857–880. https://doi.org/10.1177/0271678X241237159 (2024).
2. Shen, L. et al. Mitophagy in Cerebral Ischemia and Ischemia/Reperfusion Injury. *Front. Aging Neurosci.* **13**, 687246. https://doi.org/10.3389/fnagi.2021.687246 (2021).
3. Tuo, Q. Z., Zhang, S. T. & Lei, P. Mechanisms of neuronal cell death in ischemic stroke and their therapeutic implications. *Med. Res. Rev.* **42** (1), 259–305. https://doi.org/10.1002/med.21817 (2022).
4. Ajoolabady, A. et al. Targeting autophagy in ischemic stroke: From molecular mechanisms to clinical therapeutics. *Pharmacol. Ther.* **225**, 107848. https://doi.org/10.1016/j.pharmthera.2021.107848 (2021).
5. Lu, Y. et al. Cellular mitophagy: Mechanism, roles in diseases and small molecule pharmacological regulation. *Theranostics* **13** (2), 736–766. https://doi.org/10.7150/thno.79876 (2023).
6. Giorgi, C. et al. Mitochondria and Reactive Oxygen Species in Aging and Age-Related Diseases. *Int Rev. Cell. Mol. Biol* **340**:209–344. https://doi.org/10.1016/bs.ircmb.2018.05.006(2018).
7. Song, M., Zhou, Y. & Fan, X. Mitochondrial Quality and Quantity Control: Mitophagy Is a Potential Therapeutic Target for Ischemic Stroke. *Mol. Neurobiol.* **59** (5), 3110–3123. https://doi.org/10.1007/s12035-022-02795-6((2022).
8. Zhang, H. et al. Bioinformatics and Network Pharmacology Identify the Therapeutic Role and Potential Mechanism of Melatonin in AD and Rosacea. *Front. Immunol.* **12**, 756550. https://doi.org/10.3389/fimmu.2021.756550 (2021).
9. Sturm, D. et al. Multiomic neuropathology improves diagnostic accuracy in pediatric neuro-oncology. *Nat Med* **29**(4):917–926. https://doi.org/10.1038/s41591-023-02255-1(2023).
10. Jia, Z. et al. MAM-mediated mitophagy and endoplasmic reticulum stress: the hidden regulators of ischemic stroke. *Front. Cell. Neurosci.* **18**, 1470144. https://doi.org/10.3389/fncel.2024.1470144 (2024).
11. Guan, R. et al. Mitophagy, a potential therapeutic target for stroke. *J. Biomed. Sci.* **25** (1), 87. https://doi.org/10.1186/s12929-018-0487-4((2018).
12. Perrone, M. et al. Calcium Homeostasis in the Control of Mitophagy. *Antioxid. Redox Signal.* **38** (7–9), 581–598. https://doi.org/10.1089/ars.2022.0122 (2023).
13. An, H., Zhou, B. & Ji, X. Mitochondrial quality control in acute ischemic stroke. *J. Cereb. Blood Flow. Metab.* **41** (12), 3157–3170. https://doi.org/10.1177/0271678X211046992 (2021).
14. Mao, Z. et al. Ligustilide ameliorates hippocampal neuronal injury after cerebral ischemia reperfusion through activating PINK1/Parkin-dependent mitophagy. *Phytomedicine* **101**, 154111. https://doi.org/10.1016/j.phymed.2022.154111 (2022).

15. Shi, R. Y. et al. BNIP3 interacting with LC3 triggers excessive mitophagy in delayed neuronal death in stroke. *CNS Neurosci. Ther.* **20** (12), 1045–1055. https://doi.org/10.1111/cns.12325 (2014).
16. He, L. et al. Application of single-cell RNA sequencing technology in liver diseases: a narrative review. *Ann. Transl Med.* **9** (20), 1598. https://doi.org/10.21037/atm-21-4824 (2021).
17. Fan, X. Y., Yin, S. & Luo, S. M. SQSTM1 and its MAP1LC3B-binding domain induce forced mitophagy to degrade mitochondrial carryover during mitochondrial replacement therapy. *Autophagy* **19** (1), 363–364. https://doi.org/10.1080/15548627.2022.2077552 (2023).
18. Tang, Y. et al. PARP14 inhibits microglial activation via LPAR5 to promote post-stroke functional recovery. *Autophagy* **17** (10), 2905–2922. https://doi.org/10.1080/15548627.2020.1847799 (2021).
19. Geisler, S., Vollmer, S., Golombek, S. & Kahle, P. J. The ubiquitin-conjugating enzymes UBE2N, UBE2L3 and UBE2D2/3 are essential for Parkin-dependent mitophagy. *J. Cell. Sci.* **127** (Pt 15), 3280–3293. https://doi.org/10.1242/jcs.146035 (2014).
20. Bertolin, G. et al. The TOMM machinery is a molecular switch in PINK1 and PARK2/PARKIN-dependent mitochondrial clearance. *Autophagy*. **9**(11):1801–1817. (2013). https://doi.org/10.4161/auto.25884
21. Tiwari, S., Singh, A., Gupta, P. & Singh, K. A. UBA52 Attunes VDAC1-Mediated Mitochondrial Dysfunction and Dopaminergic Neuronal Death. *ACS Chem. Neurosci.* **14** (5), 839–850. https://doi.org/10.1021/acschemneuro.2c00579 (2023).
22. Gan, Y. et al. Ischemic neurons recruit natural killer cells that accelerate brain infarction. *Proc. Natl. Acad. Sci. U S A.* **111** (7), 2704–2709. https://doi.org/10.1073/pnas.1315943111 (2014).
23. Chen, C., Ai, Q. D., Chu, S. F., Zhang, Z. & Chen, N. H. NK cells in cerebral ischemia. *Biomed. Pharmacother.* **109**, 547–554. https://doi.org/10.1016/j.biopha.2018.10.103 (2019).
24. Parrella, E., Porrini, V., Benarese, M. & Pizzi, M. The Role of Mast Cells in Stroke. *Cells* **8** (5). https://doi.org/10.3390/cells8050437 (2019).
25. Yan, W. et al. Isolation of a novel member of small G protein superfamily and its expression in colon cancer. *World J. Gastroenterol.* **9** (8), 1719–1724. https://doi.org/10.3748/wjg.v9.i8.1719 (2003).
26. Ma, Q., Wu, X., Wu, J., Liang, Z. & Liu, T. SERP1 is a novel marker of poor prognosis in pancreatic ductal adenocarcinoma patients via anti-apoptosis and regulating SRPRB/NF-kappaB axis. *Int. J. Oncol.* **51** (4), 1104–1114. https://doi.org/10.3892/ijo.2017.4111 (2017).
27. Lim, K. M., Hwang, J. & Koh, H. C. CK2alpha Regulates Endoplasmic Reticulum Stress-Mediated Mitophagy via the PERK/ATF4/CHOP Pathway in Rotenone-Treated SH-SY5Y Cells. *Mol Neurobiol* **63**(1):69. https://doi.org/10.1007/s12035-025-05441-z(2025).
28. Lan, R. et al. Mitophagy is activated in brain damage induced by cerebral ischemia and reperfusion via the PINK1/Parkin/p62 signalling pathway. *Brain Res. Bull* **142**:63–77. https://doi.org/10.1016/j.brainresbull.2018.06.018(2018).
29. Ren, N. et al. ATP5J regulates microglial activation via mitochondrial dysfunction, exacerbating neuroinflammation in intracerebral hemorrhage. *Front. Immunol.* **15**, 1509370. https://doi.org/10.3389/fimmu.2024.1509370 (2024).
30. Kim, J., Kundu, M., Viollet, B. & Guan, K. L. AMPK and mTOR regulate autophagy through direct phosphorylation of Ulk1. *Nat. Cell. Biol.* **13** (2), 132–141. https://doi.org/10.1038/ncb2152 (2011).
31. Li, J. et al. Targeting neuronal mitophagy in ischemic stroke: an update. *Burns Trauma.* **11**, tkad018. https://doi.org/10.1093/burnst/tkad018 (2023).
32. Planas-Serra, L. et al. Sphingolipid desaturase DEGS1 is essential for mitochondria-associated membrane integrity. *J. Clin. Invest.* **133** (10). https://doi.org/10.1172/JCI162957 (2023).
33. Vos, M. et al. Ceramide accumulation induces mitophagy and impairs beta-oxidation in PINK1 deficiency. *Proc. Natl. Acad. Sci. U S A.* **118** (43). https://doi.org/10.1073/pnas.2025347118 (2021).
34. Jacobs, J. et al. A missing enzyme-rescue metabolite as cause of a rare skeletal dysplasia. *Nature* **646**(8083):218–226. https://doi.org/10.1038/s41586-025-09397-x(2025).
35. Babu, M., Singh, N. & Datta, A. In Vitro Oxygen Glucose Deprivation Model of Ischemic Stroke: A Proteomics-Driven Systems Biological Perspective. *Mol Neurobiol* **59**(4):2363–2377. https://doi.org/10.1007/s12035-022-02745-2(2022).
36. Han, B. et al. Microglial PGC-1alpha protects against ischemic brain injury by suppressing neuroinflammation. *Genome Med* **13**(1):47. https://doi.org/10.1186/s13073-021-00863-5(2021).
37. Sheng, B. et al. Exosomes-mediated delivery of miR-486-3p alleviates neuroinflammation via SIRT2-mediated inhibition of mitophagy after subarachnoid hemorrhage. *Stroke Vasc Neurol.* **10** (3), 335–346. https://doi.org/10.1136/svn-2024-003509 (2025).
38. Basak, B. & Holzbaur, E. L. F. Mitophagy in Neurons: Mechanisms Regulating Mitochondrial Turnover and Neuronal Homeostasis. *J. Mol. Biol.* **437** (18), 169161. https://doi.org/10.1016/j.jmb.2025.169161 (2025).
39. Wang, J. et al. Microglia Mitochondrial Metabolism in Neurological Diseases. *Mol. Neurobiol.* **63** (1), 337. https://doi.org/10.1007/s12035-025-05640-8 (2026).
40. Li, W. et al. Cuproptosis-related gene identification and immune infiltration analysis in systemic lupus erythematosus. *Front. Immunol.* **14**, 1157196. https://doi.org/10.3389/fimmu.2023.1157196 (2023).
41. Bai, C. et al. Identification of immune-related biomarkers for intracerebral hemorrhage diagnosis based on RNA sequencing and machine learning. *Front. Immunol.* **15**, 1421942. https://doi.org/10.3389/fimmu.2024.1421942 (2024).
42. Langfelder, P. & Horvath, S. WGCNA: an R package for weighted correlation network analysis. *BMC Bioinform.* **9**, 559. https://doi.org/10.1186/1471-2105-9-559 (2008).
43. Wang, F., Wang, B., Long, J., Wang, F. & Wu, P. Identification of candidate target genes for endometrial cancer, such as ANO1, using weighted gene co-expression network analysis. *Exp. Ther. Med.* **17** (1), 298–306. https://doi.org/10.3892/etm.2018.6965 (2019).
44. Ravasz, E., Somera, A. L., Mongru, D. A., Oltvai, Z. N. & Barabasi, A. L. Hierarchical organization of modularity in metabolic networks. *Science* **297** (5586), 1551–1555. https://doi.org/10.1126/science.1073374 (2002).
45. Turhon, M. et al. An immunogenic cell death-related regulators classification patterns and immune microenvironment infiltration characterization in intracranial aneurysm based on machine learning. *Front. Immunol.* **13**, 1001320. https://doi.org/10.3389/fimmu.2022.1001320 (2022).
46. Granata, V. et al. Contrast MR-Based Radiomics and Machine Learning Analysis to Assess Clinical Outcomes following Liver Resection in Colorectal Liver Metastases: A Preliminary Study. *Cancers (Basel).* **14**(5). (2022). https://doi.org/10.3390/cancers14051110
47. Pan, B. et al. Predicting mitophagy-related genes and unveiling liver endothelial cell heterogeneity in hepatic ischemia-reperfusion injury. *Front. Immunol.* **15**, 1370647. https://doi.org/10.3389/fimmu.2024.1370647 (2024).
48. Newman, A. M. et al. Robust enumeration of cell subsets from tissue expression profiles. *Nat. Methods.* **12** (5), 453–457. https://doi.org/10.1038/nmeth.3337 (2015).
49. Zeng, D. et al. IOBR: Multi-Omics Immuno-Oncology Biological Research to Decode Tumor Microenvironment and Signatures. *Front. Immunol.* **12**, 687975. https://doi.org/10.3389/fimmu.2021.687975 (2021).
50. Lin, W. et al. Role of Calcium Signaling Pathway-Related Gene Regulatory Networks in Ischemic Stroke Based on Multiple WGCNA and Single-Cell Analysis. *Oxid. Med. Cell. Longev.* **2021** (8060477). https://doi.org/10.1155/2021/8060477 (2021).

Author contributions

ZC: Writing, Validation, Formal analysis, Visualization, Software, Methodology, investigation, Conceptualization; WS: Methodology, Writing, Funding acquisition, Resources, Supervision, Project administration, Conceptualization; YlW: Resources, Data Curation, Visualization, Investigation; MjS: Formal analysis, Validation,

Software; RyD: Resources, Investigation, Formal analysis; XF: Visualization, Investigation, Formal analysis; LW: Visualization, Investigation, writing ; ZyZ: Investigation, Formal analysis. All authors contributed to the article and approved the submitted version.

Funding
This work is supported by Scientific Research Project of Health Commission of Heilongjiang province (No. 20240303070017).

Declarations

Competing interests
The authors declare no competing interests.

Approval for human experiments
Approval was obtained from the ethics committee of The Second Affiliated Hospital of Harbin Medical University (Ethics approval number: YJSKY2025-489). The procedures used in this study adhere to the tenets of the Declaration of Helsinki. We confirm that all experiments were performed in accordance with relevant named guidelines and regulations. We confirm that informed consent was obtained from all participants and/or their legal guardians.

Additional information
Supplementary Information The online version contains supplementary material available at https://doi.org/10.1038/s41598-026-43377-z.

Correspondence and requests for materials should be addressed to W.S.

Reprints and permissions information is available at www.nature.com/reprints.

Publisher's note Springer Nature remains neutral with regard to jurisdictional claims in published maps and institutional affiliations.